

Low damage electrical modification of 4H-SiC via ultrafast laser irradiation

Minhyung Ahn,¹ Rico Cahyadi,² Joseph Wendorf,² Willie Bowen,³ Ben Torralva,⁴ Steven Yalisove,² and Jamie Phillips¹

¹Department of Electrical Engineering and Computer Science, University of Michigan, Ann Arbor, Michigan 48109, USA

²Department of Materials Science and Engineering, University of Michigan, Ann Arbor, Michigan 48109, USA

³Dow Corning Corporation, 5300 Eleven Mile Road, Auburn, Michigan 48611, USA

⁴Department of Climate and Space Sciences and Engineering, University of Michigan, Ann Arbor, Michigan 48109, USA

(Received 22 December 2017; accepted 25 March 2018; published online 11 April 2018)

The electrical properties of 4H-SiC under ultrafast laser irradiation in the low fluence regime ($<0.50 \text{ J/cm}^2$) are presented. The appearance of high spatial frequency laser induced periodic surface structures is observed at a fluence near 0.25 J/cm^2 and above, with variability in environments like in air, nitrogen, and a vacuum. In addition to the formation of periodic surface structures, ultrafast laser irradiation results in possible surface oxidation and amorphization of the material. Lateral conductance exhibits orders of magnitude increase, which is attributed to either surface conduction or modification of electrical contact properties, depending on the initial material conductivity. Schottky barrier formation on ultrafast laser irradiated 4H-SiC shows an increase in the barrier height, an increase in the ideality factor, and sub-bandgap photovoltaic responses, suggesting the formation of photo-active point defects. The results suggest that the ultrafast laser irradiation technique provides a means of engineering spatially localized structural and electronic modification of wide bandgap materials such as 4H-SiC with relatively low surface damage via low temperature processing. Published by AIP Publishing. <https://doi.org/10.1063/1.5020445>

I. INTRODUCTION

Wide bandgap (WBG) semiconductors such as silicon carbide (SiC), gallium nitride (GaN), and gallium oxide (Ga_2O_3) are characterized by high bonding strength, mechanical hardness, and high resistance to chemical and thermal stress. These properties make WBG materials highly attractive for electronics operating in harsh environments. Moreover, due to the high breakdown field and high thermal conductivity, 4H-SiC is now commercially used for power electronic devices. However, the stability of WBG semiconductors such as 4H-SiC also creates challenges in device processing. For example, in the case of n-type doping of 4H-SiC with nitrogen, very high temperature ($>1500\text{--}1600^\circ\text{C}$) is required for postimplantation annealing.¹ In addition, 4H-SiC generally requires a high doping concentration and annealing at 900°C to form ohmic contacts with various electrode metals.² Ultrafast (femtosecond pulse) laser processing is an emerging technique³ that can be used to modify the structural and electronic properties of transparent materials such as WBG semiconductors or dielectrics. Ultrafast laser pulses may be absorbed in WBG semiconductors, even for optical wavelengths below the bandgap energy of the material, due to the high peak intensity and short pulse duration⁴ where non-linear effects and generation of defects may occur. Moreover, the femtosecond pulse duration provides an opportunity for materials modification,⁵ where the ultrafast timescale is shorter than the nanosecond timescale for thermal diffusion. Thus, ultrafast laser processing reduces the heat-affected zone, providing a new precision tool for transparent materials.⁶

Mechanisms of ultrafast laser-material interactions^{7–10} are quite different from nanosecond laser-material interactions, which can be interpreted as Joule heating and classical

laser-material interactions.¹¹ One of the features of laser-material interactions is the formation of laser induced periodic surface structures (LIPSSs): sub-wavelength self-assembled periodic nanostructures that form on the material surface after laser irradiation. LIPSSs are categorized into low spatial frequency LIPSSs (LSFLs) and high spatial frequency LIPSSs (HSFLs) which formed only by ultrafast laser irradiation. Generally, the formation of LSFLs is attributed to surface plasmon polariton (SPP) coupling,^{12–14} while the formation of HSFLs at low laser fluence is attributed to optical coupling along with stress relaxation via accumulation of ultrafast laser induced point defects in the case of semiconductors.¹⁵ During ultrafast pulse irradiation, the high carrier density excited by the high peak intensity of the laser pulse causes enhanced atomic drift⁸ following modified electron-phonon coupling.⁹ The atomic movement at each lattice site results in the generation of vacancy-interstitial pairs. These point defects can diffuse to the surface and form pits and islands with consecutive pulses. The roughened surface associated with the pits and islands may support SPP along with the transient metallic state of the material from bandgap closure.^{10,16} The strong optical coupling modifies the optical absorption properties across the material and eventually forms mechanically unstable LIPSSs. After further irradiation, the mechanical stress from the point defects is released by the bifurcation of the pre-formed LIPSSs, and eventually creates the HSFLs.

In addition to structural modifications such as HSFLs, intentional generation of point defects via ultrafast laser irradiation has great potential for modifying electrical properties. The point defects can result in direct changes in electrical conduction, or serve as a conduit for the incorporation of

dopants. Ultrafast laser processing may be an attractive technique for modifying the electronic properties of semiconductors, particularly for WBG semiconductors, where modifications typically require very high temperatures, and where doping is particularly challenging. Nanosecond laser irradiation of 4H-SiC was reported to result in the surface doping of nitrogen, with the corresponding conductivity increase of five orders of magnitude.¹⁷ However, nanosecond laser irradiation resulted in severe surface damage including the formation of globules and grooves associated with the nature of thermal process. Prior studies of ultrafast laser processing of 4H-SiC have reported LIPSS formation,¹⁸ micromachining for MEMS,^{19,20} threshold reduction from surface roughness²¹ and defects,^{22,23} amorphization,^{24,25} and generation of structural defects.^{26,27} Electrical modification of 6H-SiC (metallized with aluminum) by ultrafast laser irradiation under a high fluence ($>6.7 \text{ J/cm}^2$) demonstrated a sharp decrease in resistance²⁸ from $10^{11} \Omega$ to $10^5 \Omega$, and the existence of 4.5 meV and 51.4 meV impurity levels by temperature dependent resistivity experiments.²⁹ In addition, Ni/4H-SiC interface modification by ultrafast laser irradiation was reported³⁰ for high fluences (30 J/cm^2), where the strained Ni/4H-SiC interface resulting from ultrafast laser irradiation was believed to promote the interdiffusion of Ni, Si, and C to reduce the annealing temperature of contact formation. While these results describe the potential for ultrafast laser processing of 4H-SiC, they are still limited by severe surface damage from high fluence irradiation conditions. In this work, the relationship of ultrafast laser irradiation and electrical modification is comprehensively studied in 4H-SiC. Materials properties were studied for ultrafast laser irradiation near the threshold of HSFL formation under varying laser fluence, laser polarization, and ambient gas.

II. EXPERIMENTS

Irradiation experiments were performed on n-type epitaxial 4H-SiC (Dow Corning, 11 μm thick epitaxial layer with a nominal doping concentration of $1 \times 10^{16} \text{ cm}^{-3}$ on 350 μm thick bulk substrates with a nominal doping concentration of $5 \times 10^{18} \text{ cm}^{-3}$), as well as the bulk n-type substrates without epitaxial layers. The 4H-SiC crystalline orientation was Si face ($\langle 0001 \rangle$) with 4 degrees off-axis toward $\langle 11\bar{2}0 \rangle$. Sample preparation and laser irradiation experiments are illustrated in Fig. 1. Prior to laser irradiation, mesa structures were fabricated by photolithography and dry etching, providing a means of defining and identifying regions for laser rastering. Moreover, the edge of the mesa provides a site for increased electric field intensity upon irradiation and the corresponding reduction in the threshold for HSFL formation.²¹ This provides a “seed” or nucleation site for HSFL formation with successive femtosecond pulses.^{22,23} The edge of the mesa perpendicular to the laser polarization scatters the incoming optical wave, and this scattered field provides additional momentum to couple with the SPP mode along the mesa, which is an initial condition for HSFL formation. Samples were irradiated with a Clark MXR CPA-2001 Ti:sapphire ultrafast laser ($\lambda = 780 \text{ nm}$, 150 fs pulse width, 1KHz repetition rate) with a 105 μm Gaussian beam radius, measured by

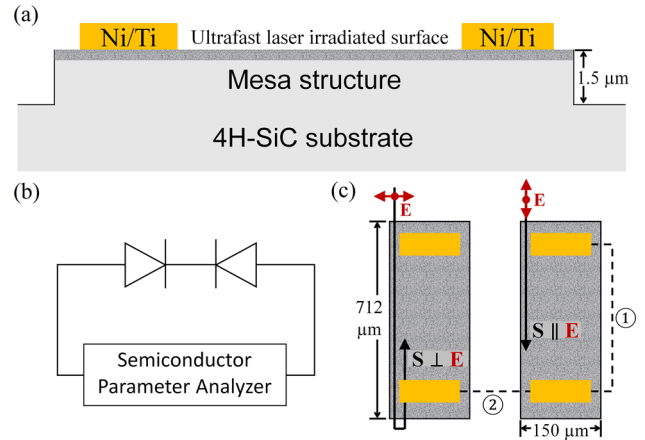


FIG. 1. Schematic illustrations of ultrafast laser irradiation experiments. (a) Lateral view of the laser irradiated SiC mesa sample with Ni/Ti contact. (b) Circuit diagram of the I-V measurements, where diode symbols indicate metal/4H-SiC interfaces as Schottky junctions. (c) Two methods of measurement for ① in-plane connection and ② out-of-plane connection. The black solid arrow represents the scanning direction (S) of the laser focal point. The red arrow represents the electric field polarization (E) of the laser for perpendicular ($S \perp E$) and parallel ($S \parallel E$) polarizations.

a DataRay WinCamD beam profiler. Rectangular areas were illuminated with variable pulse fluences and varying environments (1 atm air, 0.5 atm nitrogen, and 2.5×10^{-8} atm vacuum). With a fixed focal point, rastering was achieved by a computer controlled sample stage, as indicated in Fig. 1(c). The pulse fluence was calculated by dividing the average power of the beam measured with an Ophir Optics LLC thermal power sensor by the repetition rate. The fluence, shot separation, and polarization of the electric field can be tuned. A detailed description of the ultrafast laser system and the measurement method is provided in previous work.¹⁵ The Ti:sapphire laser rastered the mesa-fabricated 4H-SiC surface with 5 μm shot separation in the 0.2–0.5 J/cm^2 fluence range for the epitaxial 4H-SiC samples and with a 2.5 μm shot separation at 0.10–0.30 J/cm^2 for the 4H-SiC bulk substrates.

Surface morphology was studied by scanning electron microscopy (SEM, Hitachi SU8000 FE-SEM). In order to investigate the possible changes in the chemical composition and structural properties, X-ray photoelectron spectroscopy (XPS, Kratos Axis Ultra XPS system) and Raman spectroscopy (Renishaw Invia confocal micro-Raman microscopy system) were performed on select samples. Electrical contacts consisting of Ni(145 nm)/Ti(20 nm) (100 $\mu\text{m} \times 50 \mu\text{m}$) were deposited after 30 s buffered HF oxide etching and annealed at 975 °C for 5 min in a N₂/H₂ forming gas to study the electrical conductivity and the contact resistance. Typically, 4H-SiC forms a Schottky contact with Ni/Ti and may be converted to an ohmic contact with subsequent annealing (>900 °C) of 4H-SiC with a doping concentration of $>10^{18} \text{ cm}^{-3}$.² Electrical measurements were performed on a Keithley 4200 Parameter Analyzer. The metal/4H-SiC interface generally forms a Schottky barrier contact without annealing, where the electrical properties may be described by the series circuit shown in Fig. 1(b). In the case where ohmic behavior is not achieved, the current-voltage (I-V) characteristics will be limited by the reverse leakage current of the Schottky barrier. Electrical connections were considered for both in-plane and

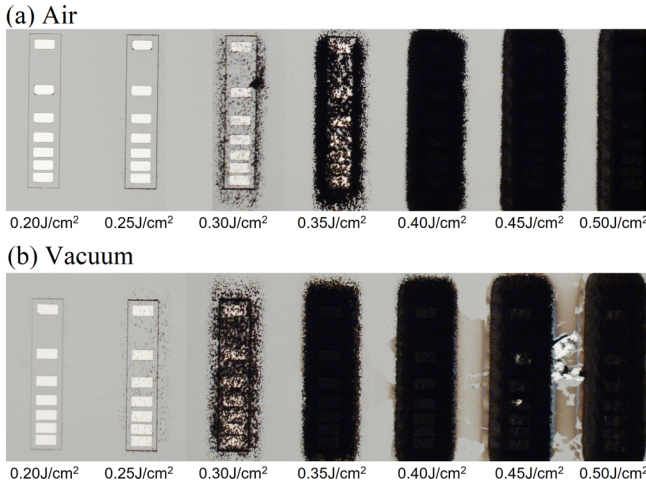


FIG. 2. Optical images of the ultrafast laser irradiated epitaxial 4H-SiC samples before annealing under various laser fluences with $5\text{ }\mu\text{m}$ shot separation and laser polarization perpendicular to the laser scanning direction ($S \perp E$). The samples were irradiated (a) in the air environment and (b) in a vacuum.

out-of-plane configurations, as shown in Fig. 1(c). For the in-plane connection, current may flow through the ultrafast laser irradiated surface, while the out-of-plane connection requires current flow through the bulk substrate material. Electrical measurements were performed before and after annealing of electrical contacts.

III. RESULTS

Ultrafast laser irradiation on the n-type 4H-SiC substrates can dramatically alter the microstructure of the material above a particular laser fluence, as shown in the optical microscopy images of Fig. 2 for irradiation in an air environment and in a vacuum. The appearance of blackened areas corresponds to optical scattering arising from the HSFL, which become apparent near 0.30 J/cm^2 and become more pronounced with

increasing fluence. A closer examination by SEM reveals the HSFL characteristics, as shown in Fig. 3, where ripples are perpendicular to the electric field polarization. The HSFL period of both environment conditions in Figs. 3(a) and 3(d) which were calculated by 2-dimensional fast Fourier transform (FFT) are similar: a 180 nm period and a 181 nm period. The HSFL period corresponds to approximately $\lambda/4$ of the center wavelength of the laser, which is similar to prior reports.^{22,31} In both air environment and under vacuum, ripples were observed from 0.20 J/cm^2 fluence, with a full coverage of the irradiated surface for 0.25 J/cm^2 fluence, indicating a threshold for HSFL formation near 0.20 J/cm^2 . From the optical images (Fig. 2) and the SEM images (Fig. 3), it is likely to conclude that certain threshold fluence for HSFL formation exists, depending on shot separation or doping concentration.

While the air environment and a vacuum show similar results for the HSFL formation threshold, the case of air environment exhibits more debris near the ripples and a shorter-range order for ripples that resemble the formation of nanograins. The distinction from the air environment may arise from the presence of oxygen and interfacial reaction with 4H-SiC during ultrafast laser irradiation. X-ray photoelectron spectroscopy (XPS) results of the surface following irradiation in the air environment at various laser fluences are shown in Fig. 4, demonstrating a clear Si-O peak in the high fluence regime (0.3 J/cm^2 and 0.4 J/cm^2).³² The observation of the Si-O peak suggests that ultrafast laser irradiation above a certain fluence in air may oxidize the 4H-SiC surface.

Ultrafast irradiation may also result in the formation of an amorphous SiC (a-SiC) layer.^{24,25} Raman spectroscopy was performed to investigate the possible changes in the crystalline structure, as shown in Fig. 5 for ultrafast laser irradiation at varying fluences under vacuum. Raman active modes labeled A_1 , E_1 , and E_2 in Fig. 5 are observed, corresponding to the wurtzite lattice structure of 4H-SiC with C_{6v} symmetry. The primary peaks of the unirradiated Raman

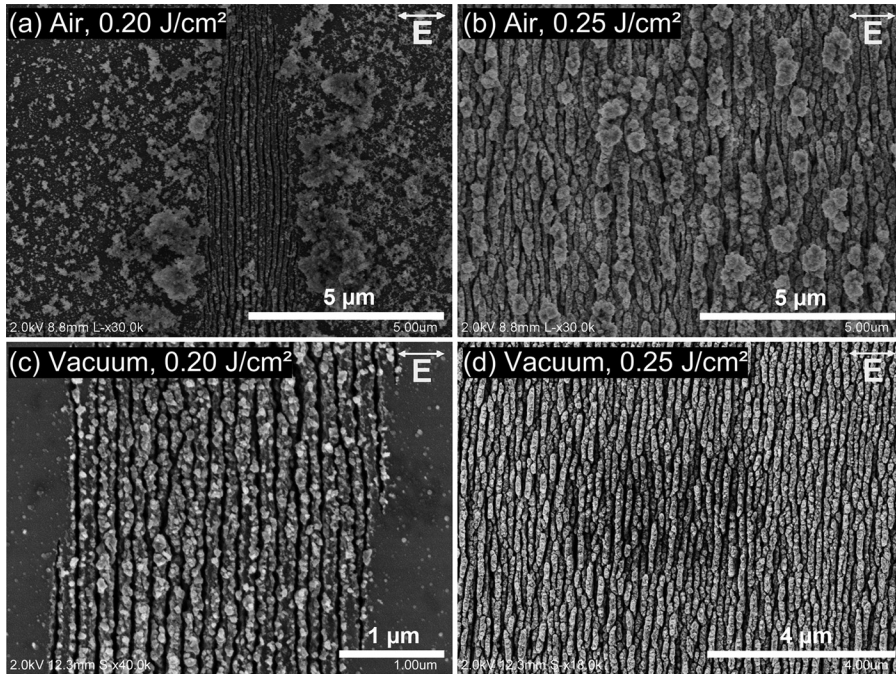


FIG. 3. SEM images of the ultrafast laser irradiated 4H-SiC substrates under different environments and laser fluences with $2.5\text{ }\mu\text{m}$ shot separation and laser polarization perpendicular to the laser scanning direction ($S \perp E$).

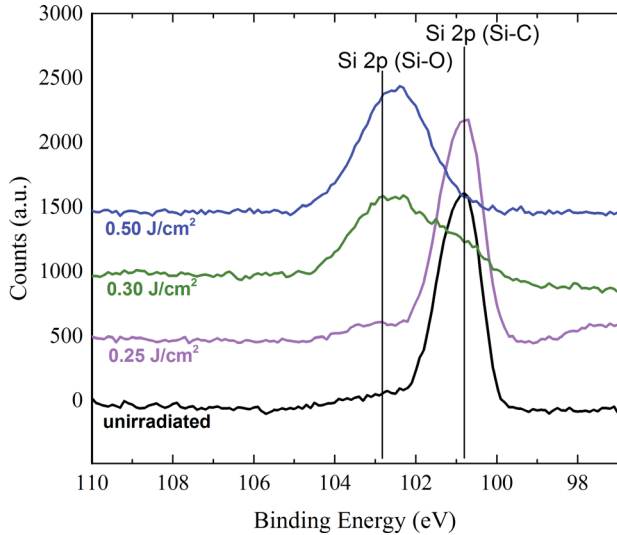


FIG. 4. XPS spectra of ultrafast laser irradiated 4H-SiC substrates in the air environment under various laser fluences. The Si 2p peak of the Si-O bond appears at 102.8 eV and the Si 2p peak of the Si-C bond appears at 100.8 eV.

spectrum of Fig. 5 agree with previously reported data^{33–35} with the exception of the unidentified peak at 985 cm^{-1} . The shape of the Raman spectra changes at fluence near 0.30 J/cm^2 and above, corresponding to the HSFL threshold observed in optical microscopy images of Fig. 2. Several broad peaks may be identified near 440 cm^{-1} , 520 cm^{-1} , 760 cm^{-1} , 910 cm^{-1} , 1410 cm^{-1} , and 1600 cm^{-1} for fluences of 0.30 J/cm^2 and 0.50 J/cm^2 . These peaks may be attributed to the Si-O bond, a-Si, highly disordered a-SiC, slightly disordered a-SiC, the D band of carbon, and the G band of carbon.³⁵ Therefore, we suggest that ultrafast laser irradiation at these fluence levels result in amorphization of the surface, similar to the report of Yamaguchi *et al.*²⁴

The current-voltage (I-V) characteristics of the epitaxial 4H-SiC material irradiated in air are shown in Fig. 6, prior to any contact annealing. The electric field polarization is perpendicular to the laser scanning direction ($S \perp E$), where

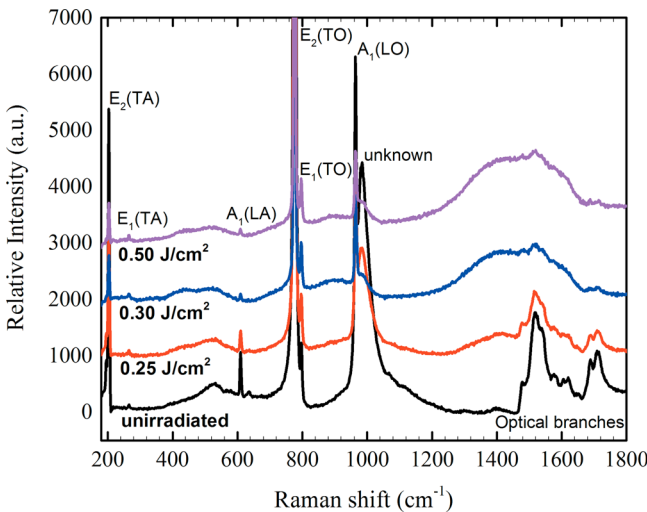


FIG. 5. Raman spectra of the ultrafast laser irradiated epitaxial 4H-SiC samples in a vacuum under various laser fluences. The peaks with marking are $E_2(\text{TA})$, 208 cm^{-1} ; $E_1(\text{TA})$, 270 cm^{-1} ; $A_1(\text{LA})$, 608 cm^{-1} ; $E_2(\text{TO})$, 776 cm^{-1} ; $E_1(\text{TO})$, 798 cm^{-1} ; $A_1(\text{LO})$, 963 cm^{-1} ; and unknown, 985 cm^{-1} .

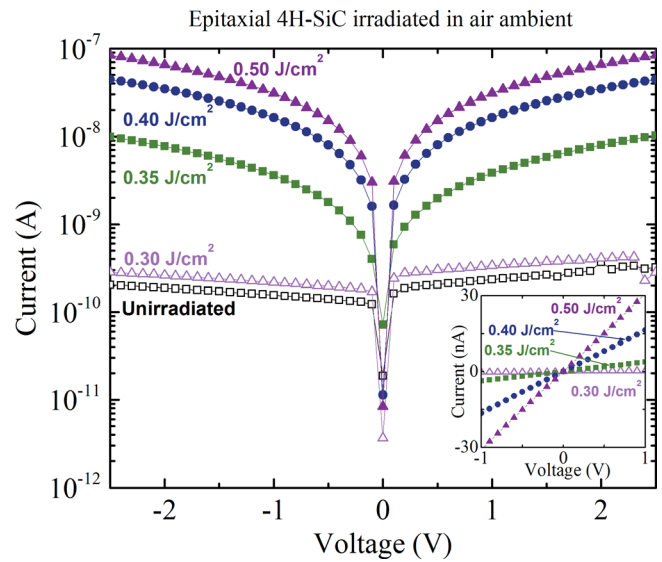


FIG. 6. I-V characteristics of the ultrafast laser irradiated epitaxial 4H-SiC in the air environment before annealing under various laser fluences with $5\text{ }\mu\text{m}$ shot separation and laser polarization perpendicular to the laser scanning direction ($S \perp E$). The inset of the figure shows the I-V characteristics in a linear scale.

current conduction would be along the HSFL ripple direction. Current flow exhibits an increase of nearly three orders of magnitude for a fluence of 0.50 J/cm^2 in comparison to the unirradiated case. There appears to be a distinct threshold for the increase in conduction between 0.30 J/cm^2 and 0.35 J/cm^2 , where the low fluence regime exhibits a behavior similar to a reverse leakage current of the Schottky barrier, while the high fluence regime exhibits linear (ohmic) behavior as can be seen in the inset of the figure. In other words, the conduction mechanism in the low fluence region may be limited by thermionic emission (with possible field- or trap-assisted processes), while conduction for the high fluence region may be limited by field emission or tunneling via interface states. The observed transition in the electrical properties near a fluence of 0.30 J/cm^2 corresponds to the HSFL threshold, where increased current flow can be explained by the formation of a conducting path near the surface. The surface conduction may be a result of donor or defect incorporation, where ultrafast laser irradiation can generate point defects that can diffuse to the surface or interfaces.¹⁵ These point defects can behave as interface trap states to enable tunneling conduction, or serve as locations for the incorporation of electrically active dopants. Alternatively, the amorphization of irradiated 4H-SiC indicated in Raman spectra of Fig. 5 may be related to the conductance increase. The a-SiC has a bandgap energy of 2.0 to 2.4 eV depending on C/Si ratio measured by optical transmission method,³⁶ and thus can alter the band structure of the laser modified region which may result in an increase in the conductance.

The conductance increase for ultrafast laser irradiation exhibits a dependence on the environment, as shown in Fig. 7. Each fluence displayed in Fig. 7 corresponds to the maximum conductance observed for each environment condition in these studies, which occurs at 0.50 J/cm^2 . The lowest conduction is observed for the case of air environment, which is

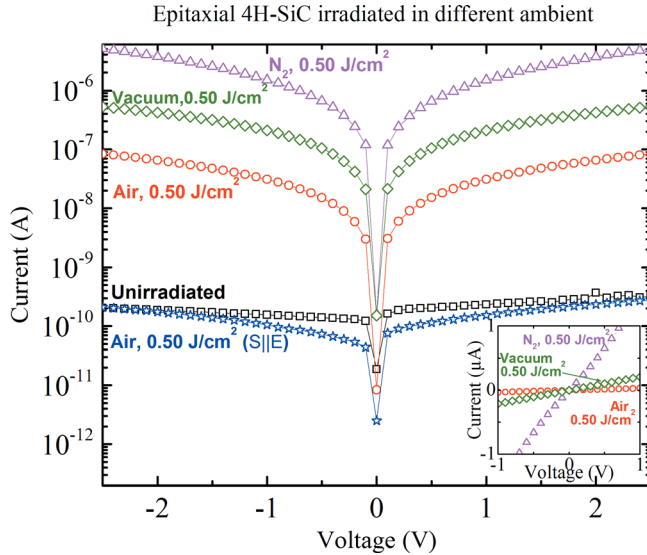


FIG. 7. I-V characteristics of the ultrafast laser irradiated epitaxial 4H-SiC before annealing under various environment conditions with $5\text{ }\mu\text{m}$ shot separation and the laser polarization perpendicular to the laser scanning direction ($S \perp E$). I-V characteristic of 0.50 J/cm^2 in air environment ($S \parallel E$) is added for comparison. The inset of the figure shows I-V characteristics in a linear scale.

likely caused by the higher degree of debris and surface damage as shown in Fig. 2, as well as the oxidation of the surface as indicated in Fig. 4. The higher conductance, for the case of nitrogen environment, may be related to possible nitrogen incorporation into the point defects of 4H-SiC generated by ultrafast laser irradiation, which can act as shallow donors.

The I-V characteristics with electric field polarization parallel to the laser scanning direction ($S \parallel E$) and the current conduction perpendicular to HSFL ripple formation show dramatically different characteristics than the ($S \perp E$) case. Despite ultrafast irradiation at high laser fluence, the current conduction does not show an appreciable difference from the unirradiated case as shown in ‘Air, 0.50 J/cm^2 ($S \parallel E$)’ of Fig. 7. This result is the opposite of prior reports on 6H-SiC by Ito *et al.*,³⁷ where ultrafast laser irradiated 6H-SiC with parallel polarization to the scanning direction had lower resistivity than the perpendicular polarization case. This substantial difference may be attributed to the vastly different laser fluence range (from 1.5 J/cm^2 to $\sim 100\text{ J/cm}^2$), where the material can be severely ablated, while this work examines a lower fluence region near the HSFL formation threshold, of approximately 0.3 J/cm^2 . The lack of electrical conduction increase for the parallel polarization condition ($S \parallel E$) may be attributed to the requirement of conduction perpendicular to the HSFL ripple direction. The depth of the modified surface properties induced by ultrafast laser irradiation may not provide full coverage over the ripple geometry, thereby preventing a complete conducting path perpendicular to the ripple direction and requiring conduction through the underlying unaltered 4H-SiC material. Moreover, the connection to the out-of-plane configuration, where there is partial conduction along the ripple direction prior to reaching the mesa edge, similarly exhibits no observable increase in conductance.

Ohmic contact formation is challenging in WBG semiconductors such as 4H-SiC, where high temperature annealing is

typically required ($>900^\circ\text{C}$),² while a lower doped material generally maintains rectifying behavior regardless of high temperature annealing. The influence of annealing on ultrafast laser irradiated low doped 4H-SiC is shown in Fig. 8 for an annealing time of 5 min at 975°C in N_2 with 5% H_2 . The annealing results in a substantial increase in the conductance for a fluence of 0.30 J/cm^2 , with approximately linear I-V behavior. Lower and higher fluence conditions do not demonstrate the same conductance increase, and also show non-linear I-V behavior. The reduction in conductance at a high fluence is likely limited by the severity of HSFL ripples and related morphological changes. For the case of ultrafast laser irradiation following annealing, optimal electrical conduction is observed near the threshold of HSFL formation (approximately 0.30 J/cm^2), corresponding to a balance between surface modification and minimization of surface damage. In addition, the conduction mechanism may be altered following the annealing, and/or limited by the characteristics of the contact. I-V characteristics with electric field polarization parallel to the laser scanning direction ($S \parallel E$) were examined for the annealed sample, and the results exhibited a similar trend to the perpendicular polarization ($S \perp E$). Moreover, the characteristics of out-of-plane connection also exhibited similar behavior. These results suggest that the annealing alters the conduction mechanism of the irradiated epitaxial 4H-SiC material from primarily surface modified conduction to limitation by the properties of the electrical contact.

The influence of ultrafast laser irradiation on electrical contact characteristics may be more carefully examined through experiments on the higher conductivity bulk 4H-SiC substrates. The fluence and environment dependence of ultrafast laser irradiation on I-V characteristics prior to any annealing are shown in Fig. 9. Similar to the results of Fig. 6 on the higher resistivity epitaxial 4H-SiC, a threshold fluence

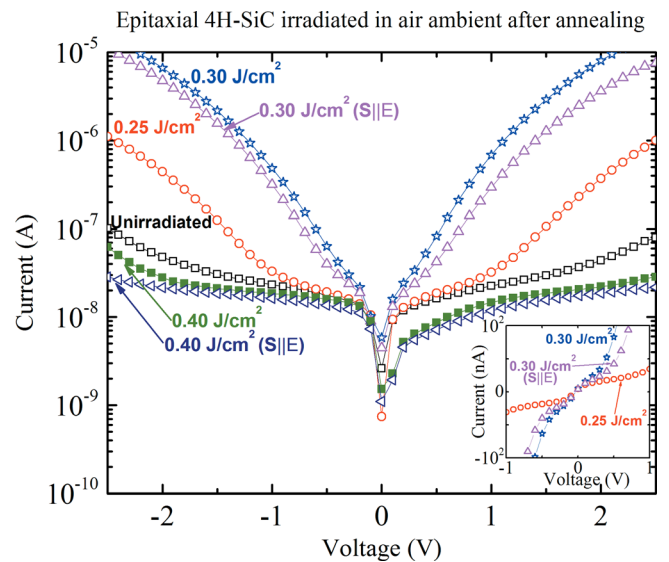


FIG. 8. I-V characteristics of the ultrafast laser irradiated epitaxial 4H-SiC in an air environment after annealing under various laser fluences with $5\text{ }\mu\text{m}$ shot separation and laser polarization perpendicular to the laser scanning direction ($S \perp E$). The same sample of Fig. 6 was used. I-V characteristics of the cases of parallel polarization ($S \parallel E$) are added for comparison. The inset of the figure shows I-V characteristics in a linear scale.

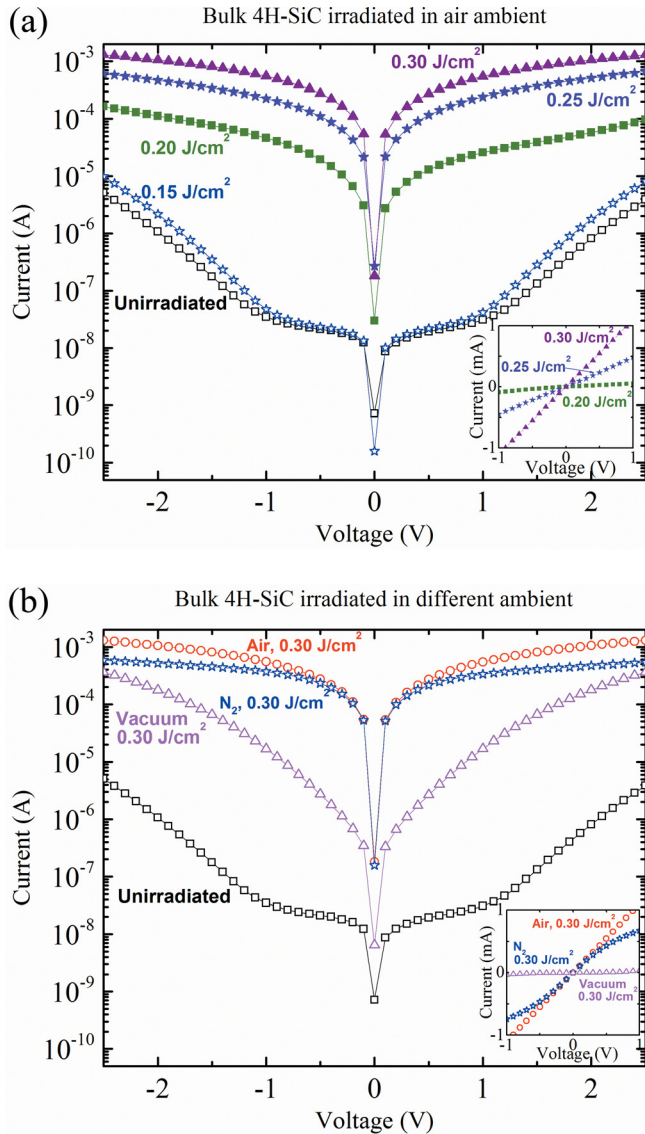


FIG. 9. I-V characteristics of the ultrafast laser irradiated bulk 4H-SiC before annealing with $2.5 \mu\text{m}$ laser shot separation and laser polarization perpendicular to the laser scanning direction ($S \perp E$) (a) under various laser fluences and (b) under various environment conditions. The inset of the figure shows I-V characteristics in a linear scale.

is observed, where conductance increases dramatically, occurring at approximately $0.20 \text{ J}/\text{cm}^2$ with relatively low surface damage. This fluence similarly corresponds to the threshold for HSFL formation, as shown in Fig. 3. The sharp increase in conductance near this threshold also corresponds to a transition from rectifying behavior to linear behavior of I-V characteristics, suggesting that ultrafast laser irradiation provides a means of ohmic contact formation without the inclusion of a thermal annealing step. The dependence of varying environment [Fig. 9(b)] shows that the varying environment results in higher conductance for air and nitrogen cases in comparison to that in vacuum, differing from the results of the higher resistivity material. This suggests that the possible effects from surface oxidation or formation of an amorphous layer are not dominating the electrical conduction for the higher conductivity material, and that it is also not a dominant factor in determining contact formation on

the ultrafast laser irradiated surface. Furthermore, the out-of-plane connection geometry for the high conductivity material demonstrates similar I-V characteristics for the in-plane geometry, suggesting that the conduction mechanism is dominated by metal-semiconductor contact formation and conduction through the bulk conducting substrate. Annealing of the high conductivity 4H-SiC samples resulted in high conductance and linear I-V behavior, regardless of irradiation (and also for the case with no ultrafast laser irradiation), and were not considered further.

IV. DISCUSSION

The qualitative electrical characteristics of ultrafast laser irradiation and annealing experiments are summarized as follows. For ultrafast laser irradiation on epitaxial 4H-SiC (higher resistivity), increased electrical conduction is observed beyond the observation of HSFL formation for the case of conduction along the ripple directions, attributed to the modification near the surface. Upon annealing, a further increase in conduction is observed (including non-irradiated samples and independent of ripple orientation), indicating that conduction becomes dominated by the characteristics of electrical contacts rather than material conductivity. Conduction on ultrafast laser irradiated bulk 4H-SiC (higher conductivity) exhibits behavior that is dominated by the characteristics of the metal-semiconductor contact and demonstrate ohmic behavior without any annealing process.

The two competing conduction mechanisms governing I-V behavior, surface conduction and contact mediated conduction are further discussed as follows. For the case of higher resistivity materials, where ultrafast laser irradiation results in measurable surface conduction differences relative to the conductivity of the starting material, the surface conduction mechanism may generally be attributed to defect formation or amorphization of the surface, as suggested by the Raman spectroscopy results (Fig. 5). The amorphized surface includes a myriad of shallow defects, which may provide a means of surface conduction via hopping conduction or trap-assisted tunneling. For higher conductivity materials, conductivity changes associated with near-surface modifications induced by ultrafast laser irradiation may not be easily resolved due to the high conductivity of the starting material. However, structural changes and/or defects induced by ultrafast laser irradiation can strongly influence electrical contact properties. Such defect formation during ultrafast laser irradiation has been suggested as an origin for HSFL formation, consisting of an accumulation of point defects at the surface and corresponding stress relaxation.¹⁵ Such crystalline point defects in 4H-SiC have generally deep levels,³⁸ which may enable defect-assisted tunneling processes at the metal/4H-SiC barrier. In the case of high-conductivity materials, the dramatic changes in Schottky barrier formation can be observed, even at relatively low fluence. The observation of ohmic behavior for ultrafast laser irradiation at $0.20 \text{ J}/\text{cm}^2$ with low surface damage [Fig. 9(a)] reveals a new opportunity of electrical modification of wide band gap materials via ultrafast laser processing.

Further exploration of these structural/electronic modifications resulting from ultrafast laser irradiated 4H-SiC was done directly on Schottky barrier devices. These experiments utilize the epitaxial 4H-SiC material, a backside Al ohmic contact on the high-conductivity substrate (without annealing) and Schottky metal contacts (Ni 145 nm/Ti 20 nm, 100 $\mu\text{m} \times 50 \mu\text{m}$) deposited on the top surface following ultrafast laser irradiation. I-V characteristics were measured in the dark and under incandescent lamp illumination as shown in Fig. 10. All the samples exhibit rectifying behavior with dark current limited by the measurement apparatus ($<10^{-13} \text{ A}$). The forward-bias characteristics may be represented by the thermionic emission model

$$I = AA^* T^2 \exp\left(-\frac{q\phi_B}{kT}\right) \left[\exp\left(\frac{q(V - IR_s)}{nkT}\right) - 1 \right], \quad (1)$$

where I , A , A^* , ϕ_B , n , V , and R_s are the current, the area of Schottky barrier contact, Richardson's constant, Schottky barrier height, the ideality factor, the voltage, and the series resistance, respectively. The theoretical value of the

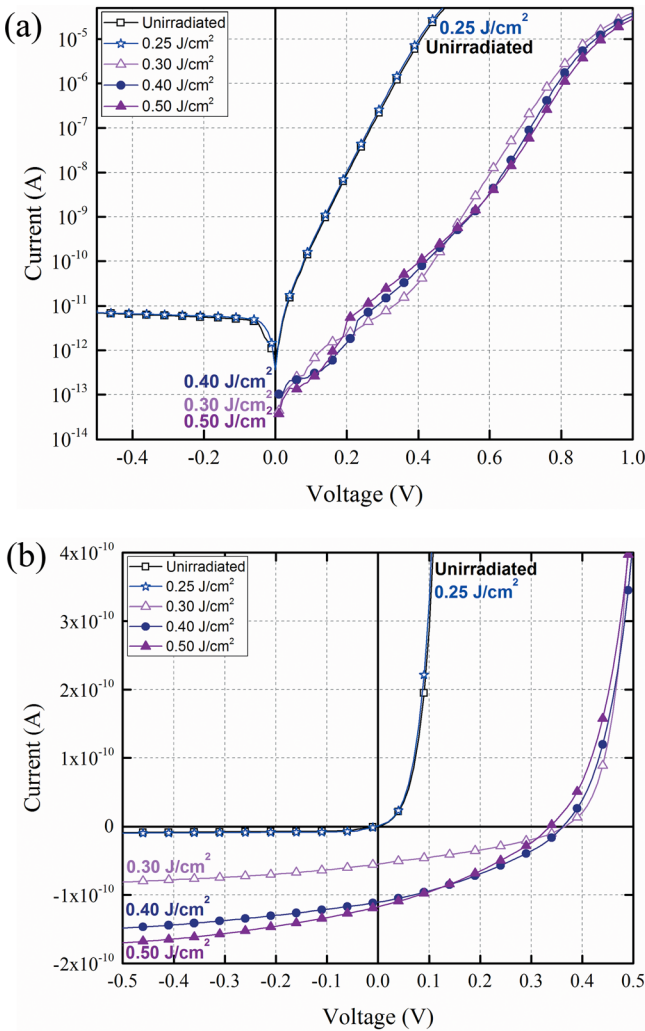


FIG. 10. I-V characteristics of Schottky diodes fabricated on epitaxial 4H-SiC after ultrafast laser irradiation in a vacuum with 5 μm laser shot separation and laser polarization parallel to the laser scanning direction ($S \parallel E$) (a) under dark conditions and (b) under incandescent lamp illumination.

Richardson's constant ($A^* = 146 \text{ A cm}^{-2}\text{K}^{-2}$) was used for data analysis.³⁹ Under dark conditions, the Schottky barrier height of the fluence regime covered by HSFLs (0.03 eV at 0.30 J/cm²) was larger than the unirradiated case (0.83 eV at 0 J/cm²) due to limited leakage current, but the ideality factor was increased from 1.09 (no irradiation) to 1.56 (at 0.30 J/cm²). The increased ideality factor suggests that non-ideal behavior such as recombination-generation in the depletion region or trap-assisted tunneling contributes to rectifying behavior. Under lamp illumination, there is non-zero current at zero voltage bias for irradiation at 0.30 J/cm², indicating the existence of photoactive states, as shown in Fig. 10(b). The extracted Schottky barrier height and the ideality factor were 0.82 eV and 1.10 without irradiation. For irradiation at 0.30 J/cm², near the HSFL threshold, the ideality factor was increased to 1.66, and a photovoltaic response was observed. The short circuit current increases with irradiation fluence, ultimately saturating near 0.40 J/cm² ($1.17 \times 10^{-11} \text{ A}$ at 0.50 J/cm²), where the HSFL fully covers the mesa. The photovoltaic response of irradiated samples suggests the formation of photoactive states responding to sub-bandgap illumination and provide further evidence for point defect formation under irradiation conditions corresponding to HSFL formation. Furthermore, optical carrier generation via states at the metal/SiC interface is highly unlikely due to optical reflection and/or absorption at the 165 nm Ni/Ti layer. Hence, it may be possible that the photovoltaic response is due to optical generation via bulk defects generated during ultrafast laser irradiation as opposed to defects at the interface between the metal and SiC. This is also consistent with the saturation at 0.4 J/cm² in Fig. 10(b), where the increased intensity will limit the absorption of ultrafast light in the bulk of SiC. This is also evident in Fig. 2, where the surface becomes black at 0.4 J/cm². Alternatively, optical carrier generation via surface states at the perimeter of the top contact may be contributing to the observed photovoltaic response.

V. CONCLUSION

Ultrafast laser irradiation of 4H-SiC exhibits pronounced modification of the structural and electronic properties of the material via an ultrafast mechanism. Electrical characteristics correlate with the formation of HSFLs, regardless of the doping concentration, annealing, and ambient gas. Conductance increases are attributed to the formation of a surface conducting path for the case of low conductivity epitaxial material in the absence of annealing. Upon annealing, conductance is found to increase by orders of magnitude, but the conduction mechanism is now limited by the properties of electrical contact. Notably, an increase in conductance was observed in the low fluence regime associated with relatively low surface damage in the case of higher conductivity materials and the ability to realize electrical contacts with ohmic behavior without thermal annealing. The characteristics of the surface properties of the ultrafast irradiated material are further observed in Schottky barrier characteristics of ultrafast laser irradiated 4H-SiC, where photoactive defects states are observed. While this

work serves as an initial demonstration of modifying the electronic materials properties of wide bandgap SiC via ultrafast laser irradiation in the low fluence regime and identification of point defect formation as the underlying physical model for this behavior, future work should be conducted to quantify the concentration, the depth distribution, and the chemical configuration of the point defects formed during ultrafast laser irradiation. The intentional structural and electronic modifications via ultrafast laser irradiation provide a novel ultrafast method of material processing for improved electrical contact formation or engineering of electronic properties.

ACKNOWLEDGMENTS

M.A. and J.P. acknowledge support from the International Consortium of Nanotechnologies (ICON) funded by Lloyd's Register Foundation, a charitable foundation which helps to protect life and property by supporting engineering-related education, public engagement and the application of research. R.C., J.W., B.T., and S.Y. acknowledge that this material is based upon work supported by the Air Force Office of Scientific Research under Award No. FA9550-16-1-0312.

- ¹T. Kimoto and J. Cooper, *Fundamentals of Silicon Carbide Technology: Growth, Characterization, Devices and Applications* (John Wiley & Sons, 2014), p. 198.
- ²S. Tanimoto, H. Okushi, and K. Arai, *Silicon Carbide* (Springer, Berlin, Heidelberg, 2004), pp. 651–669.
- ³F. Dausinger and S. Sommer, *Ultrafast Laser Processing: From Micro- to Nanoscale* (CRC Press, 2013), pp. 569–586.
- ⁴K. C. Phillips, H. H. Gandhi, E. Mazur, and S. K. Sundaram, *Adv. Opt. Photonics* **7**, 684 (2015).
- ⁵K. Sugioka and Y. Cheng, *Light: Sci. Appl.* **3**, e149 (2014).
- ⁶R. R. Gattass and E. Mazur, *Nat. Photonics* **2**, 219 (2008).
- ⁷S. Anisimov, B. Kapeliovich, and T. Perelman, *Zh. Eksp. Teor. Fiz.* **66**, 776 (1974).
- ⁸A. M. Lindenberg, *Science* **308**, 392 (2005).
- ⁹P. Stampfli and K. H. Bennemann, *Phys. Rev. B* **49**, 7299 (1994).
- ¹⁰S. K. Sundaram and E. Mazur, *Nat. Mater.* **1**, 217 (2002).
- ¹¹M. v. Allmen and A. Blatter, *Laser-Beam Interactions with Materials: Physical Principles and Applications* (Springer Science & Business Media, 2013).
- ¹²J. Bonse, S. Hohm, S. V. Kirner, A. Rosenfeld, and J. Kruger, *IEEE J. Sel. Top. Quantum Electron.* **23**, 9000615 (2017).
- ¹³J. E. Sipe, J. F. Young, J. S. Preston, and H. M. Van Driel, *Phys. Rev. B* **27**, 1141 (1983).
- ¹⁴M. Huang, F. Zhao, Y. Cheng, N. Xu, and Z. Xu, *ACS Nano* **3**, 4062 (2009).
- ¹⁵M. J. Abere, B. Torralva, and S. M. Yalisove, *Appl. Phys. Lett.* **108**, 153110 (2016).
- ¹⁶M. Schultze, K. Ramasesha, C. D. Pemmaraju, S. A. Sato, D. Whitmore, A. Gandman, J. S. Prell, L. J. Borja, D. Prendergast, K. Yabana, D. M. Neumark, and S. R. Leone, *Science* **346**, 1348 (2014).
- ¹⁷I. A. Salama, N. R. Quick, and A. Kar, *J. Electron. Mater.* **31**, 200 (2002).
- ¹⁸T. Tomita, K. Kinoshita, S. Matsuo, and S. Hashimoto, *Jpn. J. Appl. Phys., Part 2* **45**, L444 (2006).
- ¹⁹P. Molian, B. Pecholt, and S. Gupta, *Appl. Surf. Sci.* **255**, 4515 (2009).
- ²⁰Y. Dong, R. Nair, R. Molian, and P. Molian, *J. Micromech. Microeng.* **18**, 35022 (2008).
- ²¹T. Tomita, K. Kinoshita, S. Matsuo, and S. Hashimoto, *Appl. Phys. Lett.* **90**, 153115 (2007).
- ²²G. Obara, H. Shimizu, T. Enami, E. Mazur, M. Terakawa, and M. Obara, *Opt. Express* **21**, 26323 (2013).
- ²³H. Shimizu, S. Yada, G. Obara, and M. Terakawa, *Opt. Express* **22**, 17990 (2014).
- ²⁴M. Yamaguchi, S. Ueno, R. Kumai, K. Kinoshita, T. Murai, T. Tomita, S. Matsuo, and S. Hashimoto, *Appl. Phys. A: Mater. Sci. Process.* **99**, 23 (2010).
- ²⁵T. Tomita, T. Okada, H. Kawahara, R. Kumai, S. Matsuo, S. Hashimoto, M. Kawamoto, M. Yamaguchi, S. Ueno, E. Shindou, A. Yoshida, T. Tomita, R. Kumai, S. Matsuo, S. Hashimoto, T. Okada, H. Kawahara, M. Kawamoto, M. Yamaguchi, S. Ueno, E. Shindou, and A. Yoshida, *Appl. Phys. A* **100**, 113 (2010).
- ²⁶T. Okada, T. Tomita, S. Matsuo, S. Hashimoto, R. Kashino, and T. Ito, *Mater. Sci. Forum* **725**, 19 (2012).
- ²⁷Z. U. Rehman and K. A. Janulewicz, *Appl. Surf. Sci.* **385**, 1 (2016).
- ²⁸M. Deki, T. Ito, M. Yamamoto, T. Tomita, S. Matsuo, S. Hashimoto, T. Kitada, T. Isu, S. Onoda, and T. Ohshima, *Appl. Phys. Lett.* **98**, 133104 (2011).
- ²⁹M. Deki, T. Oka, S. Takayoshi, Y. Naoi, T. Makino, T. Ohshima, and T. Tomita, *Mater. Sci. Forum* **778–780**, 661 (2014).
- ³⁰T. Ueki, K. Morimoto, H. Yokota, T. Tomita, and T. Okada, *Appl. Phys. Express* **8**, 26503 (2015).
- ³¹R. Buividas, M. Mikutis, and S. Juodkazis, *Prog. Quantum Electron.* **38**, 119 (2014).
- ³²J. Binner and Y. Zhang, *J. Mater. Sci. Lett.* **20**, 123 (2001).
- ³³J. C. Burton, L. Sun, M. Poprathic, S. J. Lukacs, F. H. Long, Z. C. Feng, and I. T. Ferguson, *J. Appl. Phys.* **84**, 6268 (1998).
- ³⁴J. Burton, L. Sun, F. Long, Z. Feng, and I. Ferguson, *Phys. Rev. B* **59**, 7282 (1999).
- ³⁵S. Sorieul, J.-M. Costantini, L. Gosmain, L. Thomé, and J.-J. Grob, *J. Phys.: Condens. Matter* **18**, 5235 (2006).
- ³⁶S. Janz, *Amorphous Silicon Carbide for Photovoltaic Applications* (Universität Konstanz, 2006).
- ³⁷T. Ito, M. Deki, T. Tomita, S. Matsuo, S. Hashimoto, T. Kitada, and T. Isu, *J. Laser Micro/Nanoeng.* **7**, 16 (2012).
- ³⁸T. Kimoto and J. Cooper, *Fundamentals of Silicon Carbide Technology: Growth, Characterization, Devices, and Applications* (John Wiley & Sons, 2014), p. 133.
- ³⁹M. Sochacki, A. Kolendo, J. Szmidt, and A. Werbowy, *Solid State Electron.* **49**, 585 (2005).